Macromolecular Rapid Communication
www.mrc-journal.de

Tailoring the Cavity of Hollow Polyelectrolyte Microgels

Sarah K. Wypysek, Andrea Scotti, Mohammed O. Alziyadi, Igor I. Potemkin, Alan R. Denton, and Walter Richtering**

The authors demonstrate how the size and structure of the cavity of hollow charged microgels may be controlled by varying pH and ionic strength. Hollow charged microgels based on *N*-isopropylacrylamide with ionizable comonomers (itaconic acid) combine advanced structure with enhanced responsiveness to external stimuli. Structural advantages accrue from the increased surface area provided by the extra internal surface. Extreme sensitivity to pH and ionic strength due to ionizable moieties in the polymer network differentiates these soft colloidal particles from their uncharged counterparts, which sustain a hollow structure only at cross-link densities sufficiently high that stimuli sensitivity is reduced. Using small-angle neutron and light scattering, increased swelling of the network in the charged state accompanied by an expanded internal cavity is observed. Upon addition of salt, the external fuzziness of the microgel surface diminishes while the internal fuzziness grows. These structural changes are interpreted via Poisson–Boltzmann theory in the cell model.

S. K. Wypysek, Dr. A. Scotti
Institute of Physical Chemistry
RWTH Aachen University
52056 Aachen, Germany
E-mail: andrea.scotti@rwth-aachen.de

M. O. Alziyadi, Prof. A. R. Denton
Department of Physics
North Dakota State University
Fargo, ND 58108-6050, USA

Prof. I. I. Potemkin
Physics Department
Lomonosov Moscow State University
Moscow 119991, Russian Federation

Prof. I. I. Potemkin
DWI Leibniz Institute for Interactive Materials
52056 Aachen, Germany

Prof. I. I. Potemkin
Laboratory of Functional Materials
National Research South Ural State University
Chelyabinsk 454080, Russian Federation

Prof. W. Richtering
Institute of Physical Chemistry
RWTH Aachen University
JARA - Soft Matter Science
52056 Aachen, Germany
E-mail: richtering@rwth-aachen.de

The ORCID identification number(s) for the author(s) of this article can be found under https://doi.org/10.1002/marc.201900422.

© 2019 The Authors. Published by WILEY-VCH Verlag GmbH & Co. KGaA, Weinheim. This is an open access article under the terms of the Creative Commons Attribution License, which permits use, distribution and reproduction in any medium, provided the original work is properly cited.

DOI: 10.1002/marc.201900422

The idea of exploiting microscopic or nanoscopic soft-adaptive building blocks as a basis for novel technologies, such as drug delivery, biosensing, and responsive coatings, has matured in the last decades. Microgels are nanometer- to micrometer-sized cross-linked polymeric networks swollen in a good solvent.[1] These soft colloidal particles have emerged as pivotal model systems both for advances in the development of soft responsive materials and for studying fundamental issues regarding connections between particle internal structure and bulk phase transitions.[2]

Microgels are particularly appealing for the realization of smart materials due to their fast responsiveness to external stimuli, for example, temperature, pH, solvent composition, and electric fields.[3–5] They can exhibit a volume phase transition from a swollen soft state to a more compact and collapsed state, similar to hard incompressible colloids. Furthermore, microgels with many different shapes and architectures, including spherical, core–shell, hollow, and anisotropic microgels[6–10] can be produced with fine control of synthesis protocols.

The wide variety of such soft mesoscale objects that can be used as building blocks for smart materials arouses interest in the fundamental understanding of the structure of microgels and also facilitates a broad range of applications. Microgels find use in membranes to implement thermo-responsive permeability,[11] in biosensors to screen and capture pesticides,[12] and in matrices for guided cell growth.[13]

Another option to further enrich the range of stimuli to which microgels are responsive is the co-polymerization of different monomers during synthesis. This approach has significantly improved the use of microgels as promising candidates for controlled drug delivery systems. Multi-responsive microgels can be designed, allowing for triggered uptake and release of guest molecules by changing pH, salt concentration, or electrochemical conditions.[14–17]

Moreover, the capability to synthesize hollow microgels, polymeric cross-linked networks with a solvent-filled cavity in their center, represents another milestone for the application of microgels as nanocontainers.[18–20] The presence of a cavity increases the capacity of the network to take up small molecules, while also increasing the surface area exposed to the solvent.[21,22] Recent structural characterization of hollow poly(*N*-isopropylacrylamide) (PNIPAM) and poly(*N*-isopropylmethacrylamide) (PNIPMAM) microgels using small-angle neutron scattering (SANS) demonstrates that polymer chains

 © 2019 The Authors. Published by WILEY-VCH Verlag GmbH & Co. KGaA, Weinheim

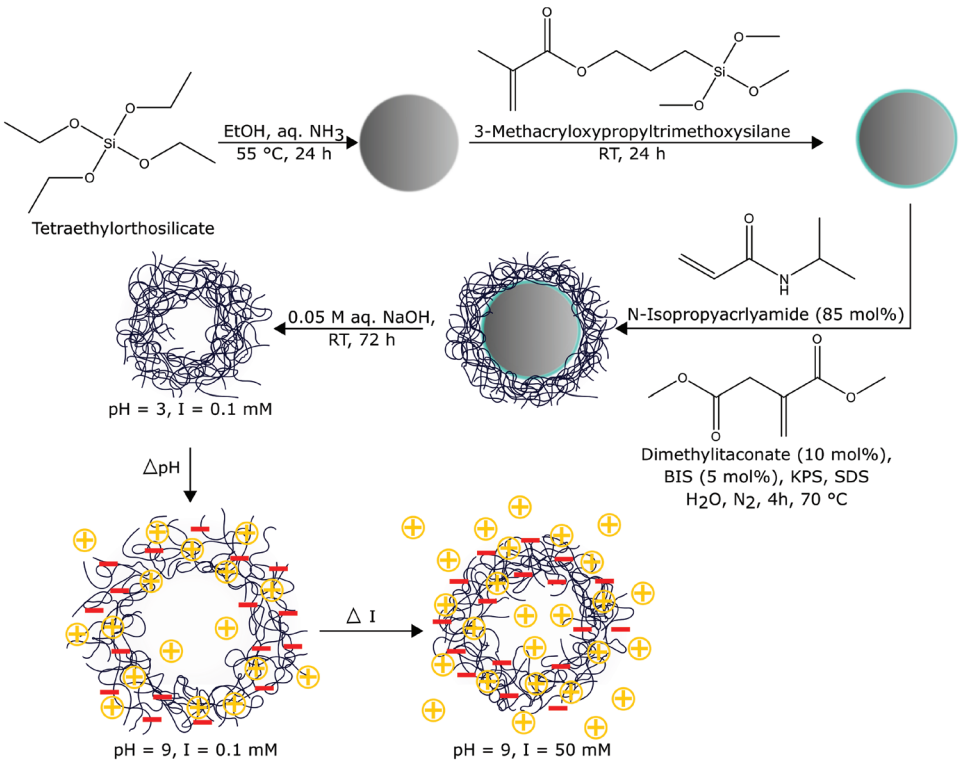

Scheme 1. Schematic synthesis of hollow anionic microgels: Starting with the synthesis and functionalization of silica cores, an uncharged poly(*N*-isopropylacrylamide-*co*-dimethylitaconate) shell is added. NaOH is used to etch the silica and saponify the ester groups. Variations in pH and ionic strength change the swelling of the microgels.

partially occupy the cavity after the dissolution of the sacrificial silica core. It has also been shown that increasing the concentration of cross-linking agent used during the synthesis (>10 mol%) enlarges the internal cavity, albeit with the unappealing consequence of reducing stimuli sensitivity.[20,23]

Concerning applications such as capsules, it is naturally essential to preserve both the inner cavity of hollow microgels and their responsiveness to external stimuli. Furthermore, the use of these nanocarriers in biological systems implies their immersion in overcrowded environments, for example, in cell membranes. Recent studies of neutral hollow microgels reveal that the cavity persists but contracts due to adsorption to solid interfaces.[24]

One possibility to further enrich the properties of hollow microgels is the introduction of monomers during the synthesis that enforce the resistance of the cavity. Indeed, it is well known that co-polymerization of PNIPAM with ionizable comonomers enhances the responsive swelling of the network by incorporating additional responsiveness to changes in pH or ionic strength of the surrounding medium. Moreover, switching between responsiveness to ionic strength in the charged state and responsiveness to temperature in the uncharged state can be tuned by changes in the pH value.[25]

Several techniques have been established to measure changes in the internal structure in response to external stimuli. SANS with contrast variations has proven to be a powerful method to obtain quantitative and statistically relevant data to gain fundamental insights into the internal structure of core–shell and hollow microgels.[20,23,26–30] Further scattering methods, such as static light scattering (SLS), can be used to increase the probed size range.

In the present contribution, we answer the question whether the size of the solvent-filled cavity and the swelling behavior of the polymeric network can be controlled by changing pH value, ionic strength, and temperature. To achieve this goal, we synthesize hollow microgels with ionizable moieties based on a co-polymer of PNIPAM and poly(itaconic acid) (p(NIPAM-*co* IA)) and investigate the response of their internal structure to different stimuli. The synthesis of hollow anionic microgels is depicted schematically in **Scheme 1**.

Combining SANS with contrast variation and light scattering, we observe an enlargement of the cavity upon ionization of the polymeric network and preservation of the cavity above the volume phase transition temperature (VPTT). Moreover, the fuzzy internal and external surfaces of the microgel network can be tuned by changing the ionic strength and thus the Debye screening length of the system. Addition of salt shortens the Debye length and enhances screening of electrostatic interactions between charges. The polymer network responds with a reduction of external surface fuzziness, whereas the fuzziness of the cavity wall increases, as illustrated in Scheme 1. This behavior implies a nonuniform distribution of counterions throughout the microgel. To verify whether changing the ionic strength affects the ion distribution inside hollow microgels, we compute the total microion density, the local Debye screening length, and the microgel electrostatic osmotic pressure for hollow, uniformly charged, spherical shells using Poisson–Boltzmann theory implemented in the spherical cell model.[31] Within our coarse-grained model, despite neglecting the detailed polymeric structure of the microgels, we predict

© 2019 The Authors. Published by WILEY-VCH Verlag GmbH & Co. KGaA, Weinheim

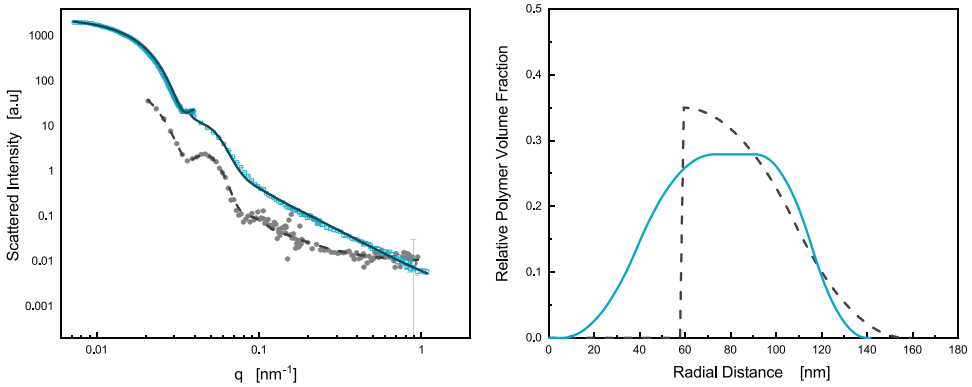

Figure 1. Scattering curves (left) and relative polymer volume fraction (right) of the core–shell microgel (gray circles and gray dashed line) compared to the hollow microgel in its uncharged state at pH = 3 and ionic strength I = 10 mM (blue circles and blue solid line) with corresponding form factor fits (lines).

a qualitative trend for the variation of Debye screening length with the bulk salt concentration that supports our hypothesis and rationalizes the experimental findings.

For the synthesis of hollow anionic microgels, we start with precursor core–shell microgels based on a sacrificial silica core.[32] Small-angle x-ray scattering (SAXS) (Figure S3, Supporting Information) reveals a radius of 59 nm for the silica cores. For the shell, a co-polymer of 85 mol% NIPAM and 10 mol% dimethylitaconate (DMI) was chosen. The cross-linking density was set to 5 mol%. The usage of uncharged co-monomers is crucial to ensure colloidal stability of the silica cores during the synthesis. For this reason, itaconic acid (IA) was chosen as the co-monomer, since it can be co-polymerized in the form of its uncharged derivative DMI. Moreover, IA has the advantage of providing a high charge density compared to co-monomers with only one ionizable group. IA is a frequently used co-monomer for microgel syntheses and thus allows comparison to other studies in the literature.[14,15]

Multi-angle dynamic light scattering (DLS) is used to measure the diffusion coefficient and to obtain the hydrodynamic radius R_h of the resulting core–shell microgels as a function of temperature. The samples were highly diluted to ensure free movement of the charged microgels in solution. The detailed evaluation of these measurements is presented in Figure S9, Supporting Information. Briefly, the core–shell microgels swell to R_h = 185 ± 1 nm in a solvent composed of 62 wt% D_2O and 38 wt% H_2O at 20 °C. The microgels undergo a volume phase transition at T = 34 °C. At 40 °C, the R_h has a value of 119 ± 1 nm.

We applied SANS to probe the structure of the resulting core–shell microgels at temperatures of 20 and 40 °C, well below and well above the VPTT (32 °C). SANS allows for contrast matching parts of hybrid materials. By choosing a solvent composition of 62 wt% D_2O and 38 wt% H_2O, the scattering length density of the silica core matches the background so that the structure of the polymeric network can be elucidated.[20] The resulting scattering curves and corresponding relative polymer volume fractions are shown in Figure S5, Supporting Information. The SANS data were fitted using the software *FitIt!* and the implemented fuzzy core–shell model.[33] This model describes the radial density profile of microgels by an inner and outer box profile convoluted with a Gaussian decay accounting for the internal and external fuzziness σ_{in} and σ_{ex}. Briefly, R_{in} represents the radius of the core, w_s gives the width of the shell. The size polydispersity is accounted for by σ_p and the correlation length by ξ. A constant background is added to account for the incoherent scattering. Finally, the model is convoluted with the resolution of the instrument. Since the core is either occupied by the solvent or its scattering length density is contrast matched with the solvent, the contrast of the core is set to 0. Parameter optimization is achieved by minimizing χ^2.[20,23] A sharp internal interface indicates the stiff silica core on the inside. The polymer network changes from highly swollen (R_o = 157 ± 8 nm) with pronounced surface fuzziness at low temperature to a dense, collapsed state (R_o = 90 ± 5 nm) with vanishing surface fuzziness. This behavior is in agreement with prior studies.[20,23,27]

Subsequent treatment of the core–shell microgels with sodium hydroxide leads to the dissolution of the silica cores and the incorporation of ionizable moieties into the polymeric network due to the saponification of the ester groups. The complete dissolution of any silica residuals can be proved by elemental mapping of silica using transmission electron microscopy (TEM), as was already shown elsewhere.[23] **Figure 1** compares the scattering curves and corresponding polymer density profiles of the core–shell microgel and the hollow microgel in its uncharged state at pH = 3 and I = 10 mM. All scattering data for the hollow microgels presented in this paper were obtained from SLS up to q = 0.04 nm^{-1} and from SANS at higher q-values. In the plotted scattering curves, the SLS data are shifted upward to merge the curves. All radial density profiles were obtained from fits to the SANS data using the fuzzy core–shell model.

The main difference between these two profiles is the expansion of the polymer toward the interior (into the cavity) once the core is dissolved, due to the removed constraint. While the internal surface is sharp for the core–shell microgel, due to the distinct surface of the rigid silica core, the hollow microgel exhibits an internal fuzziness comparable to that of its external surface. Based on the faster reaction kinetics of the cross-linker BIS the interior of the microgel is expected to have a higher

© 2019 The Authors. Published by WILEY-VCH Verlag GmbH & Co. KGaA, Weinheim

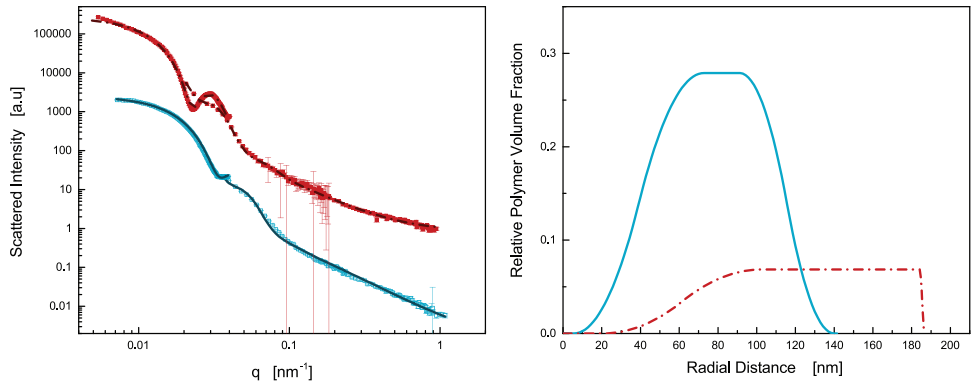

Figure 2. Scattering curves (left) and relative polymer volume fraction (right) of the hollow microgel in D_2O buffers at pH = 9 (red, filled squares) and pH = 3 (blue, open squares) and their corresponding form factor fits (pH = 9: dashed red line, pH = 3: blue line). Ionic strength was set to 10 mM and temperature was set to 20 °C. Scattering data of the sample at pH = 9 were multiplied by a factor of 100 for clarity.

cross-linking density than toward the external surface. Moreover, there might be further impacts on the polymer structure that contribute to a more complicated profile of the microgels than what we are able to resolve via SANS. Still, the model used to fit this data is sufficient to examine the trend of polymer size and density, as well as the surface fuzziness on the internal and external surfaces as already shown elsewhere.[10,23,26]

By changing the from pH = 3 to pH = 9, the acidic moieties inside the network are deprotonated, resulting in a charged network. From conductometric titrations, we calculated 2 mM charges per gram of microgel. This calculation indicates a concentration of 10 mol% itaconic acid within this microgel and deprotonation of 99 % of the acid groups of the monomer units at pH = 9. The corresponding calculations and the plot of conductivity and pH value against the volume of titrant are shown in Figure S7, Supporting Information.

The pH-dependent electrophoretic mobility, μ_E, displayed in Figure S8, Supporting Information, clearly indicates the ionization of the microgel with increasing pH. We observed a change from $\mu_E = -0.06 \times 10^{-8}$ m^2 V^{-1} s^{-1} in the neutral state at pH = 3 to $\mu_E = -1.6 \times 10^{-8}$ m^2 V^{-1} s^{-1} in the ionized state at pH = 9.

Additionally, the increase of R_h indicates the swelling of the network. This swelling is due to the presence of fixed charged groups and mobile counterions. A violation of the electroneutrality of the microgels is entropically favorable, allowing a significant fraction of counterions to diffuse outside of the microgels.[34] As a result, the microgels swell due to the difference in the osmotic pressure of inner and outer counterions and due to the electrostatic repulsion between fixed charged groups within the microgels.[35–37] The density profiles of the microgels in the two states, obtained via SANS, give a better understanding of the microgel structure and are shown in **Figure 2**.

The increased solvent uptake within the network leads to a swelling of the shell. This increase in size is accompanied by a decrease in polymer density and an increase in cavity size since the outer polymer pulls the network toward the outside. The thickness of the shell ($d = R_o - R_{in}$) changes from $d = 134 \pm 8$ nm to $d = 163 \pm 11$ nm. It is known that electrostatic repulsion of similarly charged groups in a polyelectrolyte microgel tends to bring the charged groups into the periphery, which is opposed by the elasticity of the microgel.[38] In other words, the charged groups are subjected to the action of an effective radial force directed from the center of mass to the periphery. Consequently, for hollow microgels, the electrostatic repulsion leads to the pushing of polymer chains out of the cavity. This, together with the outer polymer chains stretching toward the bulk, leads to an increase of the former partly filled cavity from $R_{in} = 40 \pm 2$ nm to $R_{in} = 62 \pm 4$ nm, which is obtained from the polymer density profile in Figure 2. Hence, the size of the cavity for the charged microgel is comparable to the size of the sacrificial silica core ($R_{SC} = 59 \pm 3$ nm). This means that the incorporation of charges into the polymeric network allows the preservation of the cavity of hollow microgels even in the swollen state at low temperatures and regular cross-linking densities.

Moreover, it is striking that the surface fuzziness of the ionized microgel differs for its internal and external surfaces. This behavior indicates different electrostatic forces inside the cavity compared to the bulk solution and will be discussed in more detail below.

The variation in size of the microgels as a function of temperature and ionic strength was probed using DLS. We analysed the hydrodynamic radii in the charged state at pH = 9 and in the uncharged state at pH = 3 (Figures S10 and S11, Supporting Information). The ionic strength was adjusted from $I = 0.1$ mM, over $I = 1$ mM and $I = 10$ mM to $I = 50$ mM, changing the Debye screening length from λ_D (0.1 mM) = 30 nm to λ_D (1 mM) = 10 nm, λ_D (10 mM) = 3 nm and λ_D (50 mM) = 1 nm.

The size of the charged microgels does not change upon heating at pH = 9 indicating suppression of thermo-sensitivity from 10 to 50 °C. Furthermore, the colloidal stability of the microgels is conserved over the same temperature range and at different ionic strengths (Figure S10, Supporting Information). The suppression of thermal responsiveness is based on the repulsion of charges within the polymeric network and the increased hydrophilicity of the network, resulting in stronger solvent–polymer interactions, which oppose the hydrophobic interactions. This finding is already well known in the literature for normal microgels.[39,40] Moreover, increasing the ionic strength of the solution leads to the screening of charges and results in a uniform decrease of the hydrodynamic radius from $R_h = 380 \pm 9$ nm at $I = 0.1$ mM to $R_h = 220 \pm 1$ nm at $I = 50$ mM.

In contrast, the microgels at pH = 3 undergo a volume phase transition at 30 °C for low ionic strength (Figure S11, Supporting Information). These neutral microgels show poor

© 2019 The Authors. Published by WILEY-VCH Verlag GmbH & Co. KGaA, Weinheim

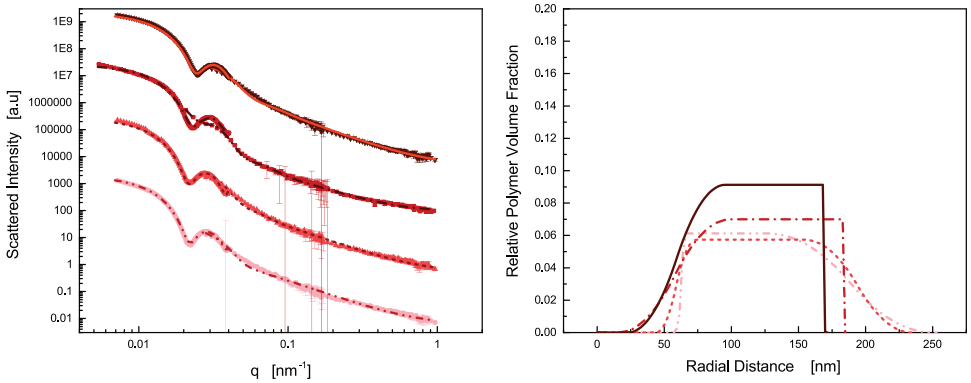

Figure 3. Scattering curves (left) and relative radial density profiles (right) of the hollow microgel in D_2O buffers at pH = 9 at different ionic strengths I = 0.1 mM, I = 1 mM, I = 10 mM, I = 50 mM (light to dark red) and their corresponding form factor fits. Temperature was set to 20 °C. Scattering data are shifted upward for clarity.

sensitivity to ionic strength below the VPTT, and hence, their initial size in the swollen state is independent of salt concentration. At high ionic strength, however, the microgels aggregate at temperatures above the VPTT.

A more detailed insight into the microgel structure as a function of ionic strength can be obtained via SLS and SANS. **Figure 3** depicts the scattered intensities and the relative polymer volume fraction of the charged microgels at pH = 9 and varying ionic strength. The density profiles (Figure 3, right) show a decrease of the overall radius, consistent with the DLS data. With decreasing radius, the polymer density increases accordingly. Based on the screening of charges upon the addition of salt to the bulk solution, the repulsion of the charged dangling polymer chains is reduced. Hence, the surface fuzziness decreases with increasing salt concentration.[41] Moreover, the addition of salt leads to a less pronounced difference in osmotic pressure between the microgel and the bulk solution and thus, allows the microgel network to expel captured solvent. As a consequence, the polymeric network is densified.

Furthermore, it can be seen that the cavity decreases as a consequence of the collapse of the outer polymer chains. However, the cavity is not filled at any ionic strength. In Figure 3 (right panel), the total microgel outer radius (R_o) is seen to decrease more strongly with increasing ionic strength than the inner radius (R_{in}), accompanied by an increase of polymer density. From the difference between the total outer radius and the inner radius of the microgel, the shell thickness can be calculated. From this calculation, we obtain a decrease of shell thickness from 191 ± 16 nm (I = 0.1 mM) to 190 ± 15 nm (I = 1 mM), 163 ± 11 nm (I = 10 mM), and finally to 147 ± 11 nm (I = 50 mM). This finding is comparable to the study of Brugnoni et al. where the outer shell of an uncharged hollow double shell microgel pulls and pushes the inner shell as a response to the swelling and collapsing of the microgel due to changes in temperature.[23]

Interestingly, the change in surface fuzziness upon the addition of salt differs for the internal and external surfaces. Along with the decrease of the Debye length, the charges are screened. The polymer network responds with a reduction of external surface fuzziness but an increase of the fuzziness toward the cavity. It has to be mentioned that both fuzzy parts of the microgel (including dangling chains) have higher swelling ability than the inner part of the microgel because of smaller cross-linking density.

To help interpret results of the scattering experiments on hollow charged microgels we applied the Poisson–Boltzmann theory in a spherical cell model.[42–44] The methods are outlined in detail in the Theoretical Methods section in the Supporting Information. We computed radial profiles of the microion number densities $n_{\pm}(r)$, the local Debye screening length $\lambda_D(r)$, and the electrostatic osmotic pressure $\Delta P_e(r)$,[45–47] as well as the average electrostatic osmotic pressure $\langle \Delta P_e \rangle$[34,48,49] over a range of ionic strengths (bulk salt concentrations).[31,44,50–53]

Note that the local Debye screening length contains no additional information, being simply proportional to the inverse square root of the microion number density. However, $\lambda_D(r)$ is a useful quantity for interpreting experimental measurements, since it directly relates to the local range of electrostatic interactions and allows for a more direct comparison with the length scales characterizing the microgel architecture. For purposes of illustration, we chose the core radius R_c = 100 nm, outer radius R_o = 180 nm, and valence $Z = 10^4$. To model dilute aqueous suspensions, we set the microgel volume fraction in the cell at a relatively low value of $\phi = (R_o/R)^3 = 0.01$ and the Bjerrum length at λ_B = 0.714 nm, appropriate for water at T = 20 °C. In order not to underestimate the radius of the cavity in the cell model, which does not include an interior fuzzy layer at the cavity wall, we chose the core radius as the largest radial distance at which the measured polymer volume fraction starts to decline, with decreasing distance from the center, from a constant value within the shell. From the SANS profiles shown in Figure 2, we estimate this distance to be roughly 100 nm. However, as a check, we also performed calculations for smaller core radii, R_c = 50 and 75 nm, and observed the same qualitative trends, as shown in Figure S14, Supporting Information.

Figure 4 (left) shows typical results for the total microion number density profiles $n_\mu(r)$. The peaks of the distributions inside the shell reflect strong attraction of counterions to the oppositely charged hydrogel, while flattening of the distributions as $r \to 0$ and $r \to R$ reflects vanishing of the electric field at the cell center and edge. With increasing ionic strength I, the microion density increases throughout the cell, including inside the cavity ($r < R_c$), indicating enhanced screening of electrostatic interactions. This trend is illustrated more directly

© 2019 The Authors. Published by WILEY-VCH Verlag GmbH & Co. KGaA, Weinheim

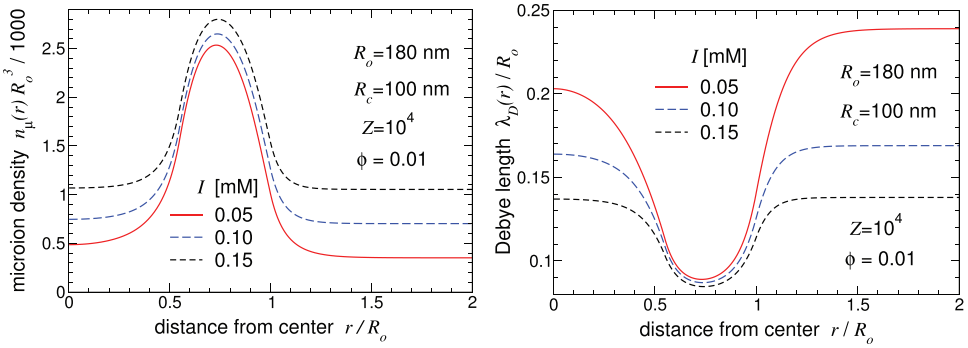

Figure 4. Total microion number density $n_\mu(r)$ (left) and local Debye screening length $\lambda_D(r)$ (Equation (2)) (right) versus distance from microgel center r (units of outer radius R_o) for microgel inner (core) radius R_c = 100 nm, outer radius R_o = 180 nm, valence $Z = 10^4$, volume fraction $\phi = 0.01$, and bulk ionic strengths I = 0.05, 0.1, and 0.15 mM.

by the plot of the local Debye screening length (Figure 4, right panel), which reaches its minimum within the shell and consistently shortens with increasing ionic strength.

We investigated the dependence of the local Debye screening length on the microgel radius R_o and the cavity radius R_c by computing $\lambda_D(r)$ for a smaller microgel (R_o = 100 nm; R_c = 20 nm) and for a larger microgel (R_o = 360 nm; R_c = 280 nm) with respect to the one reported in Figure 4. For all three cases, the thickness of the shell and the fixed charge density are kept constant. As shown in Figure S13, Supporting Information, for a given ionic strength, the ratio between the Debye lengths inside and outside the hollow microgel increases with R_o, tending to unity (i.e., same Debye length inside and outside the hollow microgel). Furthermore, for the larger microgel, the Debye lengths inside and outside the hollow microgel are virtually the same over the considered range of ionic strength, although λ_D becomes progressively shorter inside than outside as the salt concentration tends to zero. Ultimately, as the outer radius increases for fixed shell thickness, the microgel approaches the limiting case of a flat gel, where the interior and exterior environments become increasingly similar. The trend illustrated in Figure S13, Supporting Information indicates that, for a given absolute shell thickness and charge density, the larger the microgel, the smaller the relative change of the local Debye length between the inside (i.e., the cavity) and the outside, but the stronger the dependence of the interior λ_D on ionic strength. In other words, the thinner the shell relative to the outer radius, the closer the interior ionic strength is to the exterior ionic strength.

As seen in **Figure 5** (left panel), moving radially inward, the electrostatic osmotic pressure builds up and reaches a maximum within the shell, declines as the cavity wall is approached, and then remains spatially constant inside the cavity. The difference in osmotic pressure between the cavity wall ($r = R_c$) and the outer surface ($r = R_o$) reflects differing local Donnan equilibria at these two interfaces. Most importantly, with increasing ionic strength, the magnitude of $\Delta P_e(r)$ drops in both the cavity and the shell. Correspondingly, the average over the microgel volume $\langle \Delta P_e \rangle$ monotonically declines with increasing I (Figure 5, right panel).

We stress that a direct comparison between the counterion density profiles of Figure 4 or the electrostatic osmotic pressure profiles in Figure 5 and the relative polymer volume fraction in Figure 3 is not straightforward, since our idealized model does not take into account the facts that microgels are composed of polymeric chains, that they have fuzzy and less dense peripheries both inside and outside, and that their charges are not homogeneously distributed throughout the network due to different co-polymerization kinetics of the monomers. Nevertheless, even though our simple model does not account for any fuzziness of the microgel or an uneven charge distribution, the general trends of the predictions in Figures 4 and 5 confirm our hypothesis at the end of the previous section and suggest the following direct interpretation of the scattering data

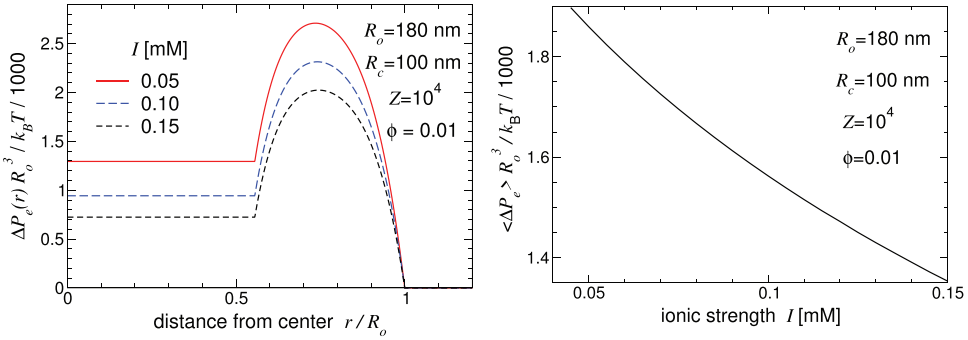

Figure 5. Left: Local electrostatic pressure $\Delta P_e(r)$ (Equation (7) versus distance from microgel center r (units of outer radius R_o) for bulk ionic strengths I = 0.05, 0.1, and 0.15 mM. Right: Average microgel electrostatic osmotic pressure $\langle \Delta P_e \rangle$ (Equation (8)) versus bulk ionic strength I. Microgel parameters are same as in Figure 4.

© 2019 The Authors. Published by WILEY-VCH Verlag GmbH & Co. KGaA, Weinheim

for polymer radial density profiles (Figure 3). With increasing ionic strength, as the electrostatic osmotic pressure drops and the local Debye screening length correspondingly shortens throughout the volume of the microgel, the charged polymers making up the gel are subject to weaker outward electrostatic repulsive forces, generated by both neighboring charged polymers and mobile microions. As a result, polymer chains near the periphery of the microgel experience a weaker outward pressure, thus becoming less stretched away from the surface and thereby reducing the outer radius. Similarly, polymer chains near the inner wall of the cavity, being likewise subject to a weaker outward pressure, become less compressed against the cavity wall and free to extend into the cavity, thereby reducing the core radius. The net result of the lowering of electrostatic osmotic pressure with increasing ionic strength is that the exterior surface of the microgel becomes less fuzzy and the interior cavity wall more fuzzy. These predicted opposing trends, reflecting the fundamental asymmetry between the interior and exterior regions, are qualitatively consistent with the SANS measurements of polymer density profiles (Figure 3), in which, with increasing I, the polymer density distribution near the periphery is seen to sharpen and contract, while the distribution near the cavity wall broadens and extends into the cavity.

Also, following the above discussion of the effect of the microgel size on the difference between the Debye lengths inside and outside the hollow microgels, we suggest that the capability to change the internal structure of hollow charged microgels by varying the ionic strength is more pronounced for microgels with radii $\lesssim 0.5$ μm. Indeed, the nanogels studied in this work display this interesting mechanism because of the combination between their nanoscale size and strong electrostatic interactions. Although we do not quantitatively analyze swelling here, the predicted dependence of the electrostatic osmotic pressure on ionic strength implies that the microgel overall deswells with increasing I, consistent with the trend of the hydrodynamic radii shown in Figure S10, Supporting Information.

In this work, we systematically investigated the influence of pH and ionic strength on the structure and swelling behavior of anionic hollow microgels. We probed the internal structure of the microgels by means of small-angle neutron and light scattering. For microgels in the uncharged state, at pH = 3, our results for the structure of the solvent-filled cavity are similar to those previously reported for hollow uncharged microgels.

By increasing the pH of the solution, we introduced charges into the polymeric network of the hollow microgels. As a result, we observed enlargement of the cavity compared to the cavity of the same microgels in the uncharged state. The size of the cavity was close to that of the precursor silica core, indicating preservation of the cavity. The finding that ionization of the network enlarges the cavity is remarkable since, for neutral microgels, preservation of the cavity is achieved mainly by increasing the cross-linker concentration, with a consequent loss in responsiveness.[20,23] However, many factors affect the internal structure of these microgels. In order to clarify synthesis conditions for the preservation of the cavity and to get a comprehensive understanding of the interplay between cross-linker content, electrostatics, total size, and cavity size, a more systematic study is needed.

At temperatures below the volume phase transition, addition of salt, and the consequent variation of ionic strength was observed to have no impact on the structure of the microgels in the uncharged state. At higher temperatures, however, the addition of salt induced aggregation of the microgels, due to the suppression of steric and electrostatic stabilization. For the charged microgels, we observed a significant decrease in their overall size upon increasing ionic strength.

Increasing the ionic strength was also observed to decrease the thickness of the fuzzy layer (due to dangling polymer chains) at the outer surface of the hollow microgels. In contrast, at the internal (cavity) surface, we observed the opposite trend. With increasing ionic strength, the fuzzy layer grew thicker due to partial extension of the polymer chains into the cavity. To explain these experimental observations, we numerically computed the microion distribution using Poisson–Boltzmann theory within the spherical cell model. We showed that increasing the ionic strength shortens the local Debye screening length throughout the microgel. As a result, the charged polymers experience a weaker electrostatic repulsion from neighboring polymers. At the same time, the electrostatic osmotic pressure, which governs swelling, decreases throughout the microgel. As a consequence, the polymer chains near the cavity wall are freer to extend, producing a more diffuse surface and shrinking the cavity. In contrast, the outward dangling chains collapse onto the microgel surface, leading to a more homogeneous and compact external structure.

We showed that a simple coarse-grained model that idealizes a hollow microgel as a charged spherical shell, without accounting for the detailed structure of the constituent polymer chains, provides a reasonable physical interpretation of the changes in microgel structure observed experimentally by SANS. More realistic models of hollow charged microgels are nevertheless needed to precisely reproduce and characterize the relation between charges, polymer density, and cross-link profile but are beyond the aim of the present contribution. In this respect, the capability of changing the internal structure of the charged hollow microgels via ionic strength constitutes the basis to validate new models for microgels in silico. This allows for better understanding of the complex interplay between the polymeric nature of the microgels and the electrostatic interaction between charges in solution and charges of the polymeric network at the relevant length scales.

Spherical charged microgels as well as neutral hollow microgels are largely used in different technological fields, for example, applied in membranes, biosensors, or delivering systems.[11,12,14,15] The combination of a hollow architecture with a charged network, that we achieved in the system presented in this study, further enrich the toolbox for altering chemical and physical features of functional microgels. The structural response of these microgels when confined at liquid–liquid interfaces or in overcrowded environments presents intriguing questions regarding the interplay between electrostatic interactions and softness and how these properties affect the phase behavior of soft charged spheres.[26,54,55] Beyond the study of fundamental properties, these microgels are also promising candidates to improve the aforementioned applications

© 2019 The Authors. Published by WILEY-VCH Verlag GmbH & Co. KGaA, Weinheim

of microgels. Still, the development of practical applications of hollow anionic microgels will require further studies, for instance, on the uptake and release of small guest molecules.

Supporting Information

Supporting Information is available from the Wiley Online Library or from the author.

All the data used for this paper are available, under request, at https://hdl.handle.net 21.11102/5f324dd9-b837-11e9-9a63-e41f1366df48.

Acknowledgements

The authors gratefully acknowledge financial support from the SFB 985 "Functional Microgels and Microgel Systems" of Deutsche Forschungsgemeinschaft within Project A3. A.S. thanks the Alexander-von-Humboldt foundation for financial support. I.I.P. acknowledges the Government of Russian Federation within Act 211, Contract No. 02.A03.21.0011 for financial support. M.O.A. thanks Shaqra University for financial support. Experiments performed at the KWS-2 instrument were operated by JCNS at Heinz Maier-Leibnitz Zentrum (MLZ) Garching, Germany and on the instrument SANS-II at SINQ, Paul Scherrer Institut. The authors thank Dr. Judith E. Houston and Dr. Urs Gasser for their help on-site during the beamtime on KWS-2 and SANS-II, respectively.

Conflict of Interest

The authors declare no conflict of interest.

Keywords

computer simulations, microgels, Poisson–Boltzmann, polyelectrolytes, scattering

Received: August 15, 2019
Revised: October 12, 2019
Published online: November 18, 2019

[1] M. Karg, A. Pich, T. Hellweg, T. Hoare, L. A. Lyon, J. J. Crassous, D. Suzuki, R. A. Gumerov, S. Schneider, I. I. Potemkin, W. Richtering, *Langmuir* **2019**, *35*, 6231.
[2] F. A. Plamper, W. Richtering, *Acc. Chem. Res.* **2017**, *50*, 131.
[3] R. Keidel, A. Ghavami, D. M. Lugo, G. Lotze, O. Virtanen, P. Beumers, J. S. Pedersen, A. Bardow, R. G. Winkler, W. Richtering, *Sci. Adv.* **2018**, *4*, eaao7086.
[4] J. D. Debord, L. A. Lyon, *Langmuir* **2003**, *19*, 7662.
[5] T. Colla, P. S. Mohanty, S. Nöjd, E. Bialik, A. Riede, P. Schurtenberger, C. N. Likos, *ACS Nano* **2018**, *12*, 4321.
[6] J. Brijitta, P. Schurtenberger, *Current Opinion in Colloid & Interface Science* **2019**, p. 87.
[7] A. P. H. Gelissen, A. Oppermann, T. Caumanns, P. Hebbeker, S. K. Turnhoff, R. Tiwari, S. Eisold, U. Simon, Y. Lu, J. Mayer, W. Richtering, A. Walther, D. Wöll, *Nano Lett.* **2016**, *16*, 7295.
[8] a) C. D. Jones, L. A. Lyon, *Macromolecules* **2000**, *33*, 8301; b) V. Städele, U. Gasser, H. Dietsch, *Soft Matter* **2012**, *8*, 4427.
[9] J. J. Crassous, A. M. Mihut, L. K. Månsson, P. Schurtenberger, *Nanoscale* **2015**, *7*, 15971.
[10] J. Dubbert, K. Nothdurft, M. Karg, W. Richtering, *Macromol. Rapid Commun.* **2015**, *36*, 159.
[11] M. Barth, M. Wiese, W. Ogieglo, D. Go, A. Kuehne, M. Wessling, *J. Membr. Sci.* **2018**, *555*, 473.
[12] a) L. V. Sigolaeva, S. Y. Gladyr, A. P. H. Gelissen, O. Mergel, D. V. Pergushov, I. N. Kurochkin, F. A. Plamper, W. Richtering, *Biomacromolecules* **2014**, *15*, 3735; b) L. V. Sigolaeva, S. Y. Gladyr, O. Mergel, A. P. H. Gelissen, M. Noyong, U. Simon, D. V. Pergushov, I. N. Kurochkin, F. A. Plamper, W. Richtering, *Anal. Chem.* **2017**, *89*, 6091.
[13] J. C. Rose, D. B. Gehlen, T. Haraszti, J. Köhler, C. J. Licht, L. D. Laporte, *Biomaterials* **2018**, *163*, 128.
[14] A. P. H. Gelissen, A. Scotti, S. K. Turnhoff, C. Janssen, A. Radulescu, A. Pich, A. A. Rudov, I. I. Potemkin, W. Richtering, *Soft Matter* **2018**, *14*, 4287.
[15] W. Xu, A. A. Rudov, R. Schroeder, I. V. Portnov, W. Richtering, I. I. Potemkin, A. Pich, *Biomacromolecules* **2019**, *20*, 1578.
[16] O. Mergel, S. Schneider, R. Tiwari, P. T. Kühn, D. Keskin, M. C. A. Stuart, S. Schöttner, M. de Kanter, M. Noyong, T. Caumanns, J. Mayer, C. Janzen, U. Simon, M. Gallei, D. Wöll, P. van Rijn, F. A. Plamper, *Chem. Sci.* **2019**, *10*, 1844.
[17] S. S. Said, S. Campbell, T. Hoare, *Chem. Mater.* **2019**, *31*, 4971.
[18] L. Zha, Y. Zhang, W. Yang, S. Fu, *Adv. Mater.* **2002**, *14*, 1090.
[19] S. Nayak, D. Gan, M. J. Serpe, L. A. Lyon, *Small* **2005**, *1*, 416.
[20] J. Dubbert, T. Honold, J. S. Pedersen, A. Radulescu, M. Drechsler, M. Karg, W. Richtering, *Macromolecules* **2014**, *47*, 8700.
[21] K. C. Bentz, D. A. Savin, *Polym. Chem.* **2018**, *9*, 2059.
[22] Y. Su, O. F. Ojo, I. K. M. Tsengam, J. He, G. L. McPherson, V. T. John, J. A. Valla, *Langmuir* **2018**, *34*, 14608.
[23] M. Brugnoni, A. Scotti, A. A. Rudov, A. P. H. Gelissen, T. Caumanns, A. Radulescu, T. Eckert, A. Pich, I. I. Potemkin, W. Richtering, *Macromolecules* **2018**, *51*, 2662.
[24] M. F. Schulte, A. Scotti, A. P. H. Gelissen, W. Richtering, A. Mourran, *Langmuir* **2018**, *34*, 4150.
[25] C. Hofzumahaus, P. Hebbeker, S. Schneider, *Soft Matter* **2018**, *14*, 4087.
[26] A. Scotti, M. Brugnoni, A. A. Rudov, J. E. Houston, I. I. Potemkin, W. Richtering, *J. Chem. Phys.* **2018**, *148*, 174903.
[27] M. Stieger, W. Richtering, J. S. Pedersen, P. Lindner, *J. Chem. Phys.* **2004**, *120*, 6197.
[28] U. Gasser, J. S. Hyatt, J.-J. Lietor-Santos, E. S. Herman, L. A. Lyon, A. Fernandez-Nieves, *J. Chem. Phys.* **2014**, *141*, 034901.
[29] P. S. Mohanty, S. Nöjd, K. Van Gruijthuijsen, J. J. Crassous, M. Obiols-Rabasa, R. Schweins, A. Stradner, P. Schurtenberger, *Sci. Rep.* **2017**, *7*, 1487.
[30] M. Cors, L. Wiehemeier, Y. Hertle, A. Feoktystov, F. Cousin, T. Hellweg, J. Oberdisse, *Langmuir* **2018**, *34*, 15403.
[31] A. R. Denton, *J. Phys.: Condens. Matter* **2010**, *22*, 364108–1–12.
[32] W. Stöber, A. Fink, E. Bohn, *J. Colloid Interface Sci.* **1968**, *26*, 62.
[33] O. L. J. Virtanen, FitIt! **2015**, https://www.github.com/ovirtanen/fitit (accessed: September 2016).
[34] A. R. Denton, Q. Tang, *J. Chem. Phys.* **2016**, *145*, 164901–1–10.
[35] A. Fernández-Nieves, A. Fernández-Barbero, B. Vincent, F. J. de las Nieves, *Macromolecules* **2000**, *33*, 2114.
[36] E. Y. Kramarenko, A. R. Khokhlov, K. Yoshikawa, *Macromolecules* **1997**, *30*, 3383.
[37] H. Kobayashi, R. Halver, G. Sutmann, R. G. Winkler, *Polymers* **2017**, *9*, 15.
[38] A. M. Rumyantsev, A. A. Rudov, I. I. Potemkin, *J. Chem. Phys.* **2015**, *142*, 171105.
[39] T. Hoare, R. Pelton, *Macromolecules* **2004**, *37*, 2544.
[40] J. P. Pinheiro, L. Moura, R. Fokkink, J. P. S. Farinha, *Langmuir* **2012**, *28*, 5802.
[41] S. Nöjd, P. Holmqvist, N. Boon, M. Obiols-Rabasa, P. S. Mohanty, R. Schweins, P. Schurtenberger, *Soft Matter* **2018**, *14*, 4150.

© 2019 The Authors. Published by WILEY-VCH Verlag GmbH & Co. KGaA, Weinheim

[42] R. A. Marcus, *J. Chem. Phys.* **1955**, *23*, 1057.
[43] H. Wennerström, B. Jönsson, P. Linse, *J. Chem. Phys.* **1982**, *76*, 4665.
[44] M. Deserno, C. Holm, in *Electrostatic Effects in Soft Matter and Biophysics* (Eds: C. Holm, P. Kékicheff, R. Podgornik), NATO Advanced Studies Institute, Series II: Mathematics Physics and Chemistry, Vol. 46, Dordrecht, Kluwer **2001**, pp. 27.
[45] E. Trizac, J.-P. Hansen, *Phys. Rev. E* **1997**, *56*, 3137.
[46] A. Widom, J. Swain, J. Silverberg, *Phys. Rev. E* **2009**, *80*, 016301–1–7.
[47] A. R. Denton, M. O, Alziyadi,*J. Chem. Phys.* **2019**, *151*, 074903–1–19.
[48] M. M. Hedrick, J. K. Chung, A. R. Denton, *J. Chem. Phys.* **2015**, *142*, 034904–1–12.
[49] Q. Tang, A. R. Denton, *Phys. Chem. Chem. Phys.* **2015**, *17*, 11070.
[50] G. C. Claudio, K. Kremer, C. Holm, *J. Chem. Phys.* **2009**, *131*, 094903–1–9.
[51] J. Landsgesell, D. Sean, P. Kreissl, K. Szuttor, C. Holm, *Phys. Rev. Lett.* **2019**, *122*, 208002–1–6.
[52] D. Ben-Yaakov, D. Andelman, D. Harries, R. Podgornik, *J. Phys.: Condens. Matter* **2009**, *21*, 424106.
[53] Y. Hallez, J. Diatta, M. Meireles, *Langmuir* **2014**, *30*, 6721.
[54] G. M. Conley, P. Aebischer, S. Nöjd, P. Schurtenberger, F. Scheffold, *Sci. Adv.* **2017**, *3*, e1700969.
[55] K. Geisel, L. Isa, W. Richtering, *Angew. Chem.* **2014**, *126*, 5005.

© 2019 The Authors. Published by WILEY-VCH Verlag GmbH & Co. KGaA, Weinheim